THE JOURNAL OF BIOLOGICAL CHEMISTRY VOL. 286, NO. 4, pp. 3104–3118, January 28, 2011

Sts1 Plays a Key Role in Targeting Proteasomes to the Nucleus*[S]

Received for publication, April 19, 2010, and in revised form, November 3, 2010 Published, JBC Papers in Press, November 12, 2010, DOI 10.1074/jbc.M110.135863

Li Chen, Lizbeth Romero, Show-Mei Chuang, Vincent Tournier, Kishore Kumar Joshi, Jung Ah Lee, Gopala Kovvali, and Kiran Madura[1]

From the Department of Biochemistry, Robert Wood Johnson Medical School, Piscataway, New Jersey 08854

The evidence that nuclear proteins can be degraded by cytosolic proteasomes has received considerable experimental support. However, the presence of proteasome subunits in the nucleus also suggests that protein degradation could occur within this organelle. We determined that Sts1 can target proteasomes to the nucleus and facilitate the degradation of a nuclear protein. Specific *sts1* mutants showed reduced nuclear proteasomes at the nonpermissive temperature. In contrast, high expression of Sts1 increased the levels of nuclear proteasomes. Sts1 targets proteasomes to the nucleus by interacting with Srp1, a nuclear import factor that binds nuclear localization signals. Deletion of the NLS in Sts1 prevented its interaction with Srp1 and caused proteasome mislocalization. In agreement with this observation, a mutation in Srp1 that weakened its interaction with Sts1 also reduced nuclear targeting of proteasomes. We reported that Sts1 could suppress growth and proteolytic defects of *rad23*Δ *rpn10*Δ. We show here that Sts1 suppresses a previously undetected proteasome localization defect in this mutant. Taken together, these findings explain the suppression of *rad23*Δ *rpn10*Δ by Sts1 and suggest that the degradation of nuclear substrates requires efficient proteasome localization.

Many factors that regulate the cell cycle, DNA repair, transcription, and tumor suppression are nuclear proteins that are degraded by the ubiquitin/proteasome system (1). However, the mechanism that mediates their turnover and the subcellular location of degradation are often not known. Nuclear proteasomes (2, 3) may perform both proteolytic and nonproteolytic functions (4, 5). The evidence that the hydrolytic activities of proteasomes are present in the nucleus is limited. Although some proteins are degraded within the nucleus (4), others are exported from the nucleus and degraded by cytosolic proteasomes (6–8). It is unknown if nuclear degradation is restricted to specific proteins, while others are exported and degraded by cytoplasmic proteasomes.

Rad23 is a substrate shuttle factor that can transfer ubiquitinated proteins to the proteasome (9, 10), whereas Rpn10 is a major proteasome receptor for multiubiquitinated proteins (11–15). The loss of both proteins in *rad23*Δ *rpn10*Δ caused severe growth and proteolytic defects, including sensitivity to drugs, stabilization of substrates, and accumulation of ubiquitinated proteins (16). Sts1 is a dosage suppressor of these pleiotropic defects of *rad23*Δ *rpn10*Δ (17), indicating that it plays a role in the ubiquitin/proteasome system. In agreement, we found that Sts1 protein can bind the proteasome, and an *sts1-2* mutant (C194Y) was defective in protein degradation and accumulated high levels of ubiquitinated proteins. Significantly, the interaction between multiubiquitinated proteins and proteasomes was reduced in *sts1-2*.

We report here that Sts1 is required for efficient translocation of proteasomes to the nucleus. We propose that the failure of proteasomes to bind multiubiquitinated substrates in *sts1-2* (17) is most likely due to reduced levels of proteasomes at the nucleus. We determined that proteasomes are also mislocalized in *rad23*Δ *rpn10*Δ, and this defect is suppressed by Sts1. The protein degradation deficiency of *rad23*Δ *rpn10*Δ is likely also caused by a failure to target proteasomes to the nucleus, which could interfere with the degradation of nuclear proteins.

Sts1 binds Srp1 (importin-α), a nuclear transport protein (18), and also forms a distinct interaction with the proteasome subunit Rpn11. It was proposed that these interactions by Sts1 mediated different functions (19). However, a specific *SRP1* mutant (*srp1-49*) harbors a defect in both protein degradation (19) and nuclear targeting of proteasomes (18). We determined that an *sts1* mutant that is unable to bind Srp1 has reduced levels of nuclear proteasomes. As expected, a nuclear localization signal (NLS) in Sts1 is required for binding Srp1 and promoting nuclear trafficking of proteasomes. In a reciprocal study, we found that a mutation in Srp1 that reduced its interaction with Sts1 was also deficient in recruiting proteasomes to the nucleus. Thus, protein degradation appears to be affected by the level of nuclear proteasomes, which is a consequence of the interaction between Srp1 and Sts1. Taken together, these genetic and biochemical studies offer insight into the mechanism of proteasome translocation to the nucleus and demonstrate that a failure causes cell death.

EXPERIMENTAL PROCEDURES

Yeast Strains and Plasmids—Yeast strains harboring mutations in *SRP1* were provided by Drs. P. Tongaonkar and M. Nomura (University of California, Irvine). DNA templates were sequenced, and the mutations were verified (*srp1-31* S116F; *srp1-49* E145K). Strains containing mutations in *STS1* were also provided by Dr. F. Wyers. Plasmids for generating

* This work was supported, in whole or in part, by National Institutes of Health Grant CA083875 (to K. M.).
[S] The on-line version of this article (available at http://www.jbc.org) contains supplemental Figs. 1 and 2.
[1] To whom correspondence should be addressed: SPH-383, 683 Hoes Lane, Piscataway, NJ 08854. Fax: 732-2355417; E-mail: maduraki@umdnj.edu.

TABLE 1

Strain	Description	Source
NA10	*MAT***a** *ura3-1, trp1-1, ade2-1, leu2-3, 112, his3-11* (*STS1*)	F. Wyers
NA25	*MAT***a** *ura3-1, trp1-1, ade2-1, leu2-3, 112, his3-11, sts1-2* (C194Y)	F. Wyers
LRY239	NA10: *PRE6*-GFP::*URA3*::*HIS3*	
LRY171	NA25: *PRE6*-GFP::*URA3*::*HIS3*	
LRY227	NA10: *RPN1*-GFP::*URA3*::*HIS3*	
LRY159	NA25: *RPN1*-GFP::*URA3*::*HIS3*	
LRY178	LRY159, 5-FOA^R	
LRY241	NA10: *RPN11*-GFP::*URA3*::*HIS3*	
LRY161	NA25: *RPN11*-GFP::*URA3*::*HIS3*	
LCY1902	LRY239 + Yeplac181 vector	
LCY1933	LRY239 + P_{CUP1}-FLAG-Sts1	
LCY1903	LRY171 + P_{CUP1}-FLAG-Sts1	
LCY1927	LRY227 + pRS vector	
LCY1928	LRY159 + pRS vector	
LCY1929	LRY159 + pRS-Sts1	
LCY1930	LRY159 + pRS-sts1$^{\Delta NLS}$	
LCY1951	LRY178 + pRS-sts1-11	
NOY388	*MAT***a**, *ade2-1, his3-11, trp1-1, ura3-1, leu2-3, −112* (*SRP1*)	M. Nomura
NOY612	*MAT***a**, *ade2-1, his3-11, trp1-1, ura3-1, leu2–3, −112* (*srp1-31*: S116F)	M. Nomura
NOY613	*MAT***a**, *ade2-1, his3-11, trp1-1, ura3-1, leu2-3, −112* (*srp1-49*: E145K)	M. Nomura
LRY223	NOY388: *RPN1*-GFP::*URA3*::*HIS3*	
LRY224	NOY612: *RPN1*-GFP::*URA3*::*HIS3*	
LRY225	NOY613: *RPN1*-GFP::*URA3*::*HIS3*	
LRY203	*RAD23 RPN10*::*RPT1* -GFP::*URA3*::*HIS3*, 5-FOA^R	16
LRY189	*rad23*Δ *rpn10*Δ::*RPT1*-GFP::*URA3*::*HIS3*, 5-FOA^R	16
LCY2011	LRY189 + P_{GAL}-*STS1*	
LCY2087	NA10: *CLB2-HA*::*TRP1*	
LCY2088	NA25: *CLB2-HA*::*TRP1*	
MHY501	*MATα his3-200, leu2-2, 112, ura3-52, lys2-801, trp1-1*	M. Hochstrasser
MHY553	*MATα his3-200, leu2-2, 112, ura3-52, lys2-801, trp1-1, ubc6*Δ::*HIS3 ubc7*Δ::*URA3*	M Hochstrasser

TABLE 2

Plasmid	Description	Source
LEP164	P_{CUP1}-FLAG-*STS 1*	9
LEP297	P_{CUP1}-FLAG-*sts1–2* (C194Y)	9
DEP177	P_{GAL}-*STS1*	9
pNOY470	pRS-Sts1	M. Nomura
pNOY480	pRS-sts1$^{\Delta NLS}$	M. Nomura
pNOY343	pRS-sts1–11 (E43G)	M. Nomura
LEP262	pBSHU-Rpn1-GFP-HA	C. Enenkel
LEP263	pBSHU-Rpt1-GFP-HA	C. Enenkel
LEP264	pBSHU-Rpn11-GFP-HA	C. Enenkel
LEP269	pBSHU-Pre6-GFP-HA	C. Enenkel
LEP163	pGEX-Sts1	
LEP606	pGEX-sts1–2	
LEP633	pGEX-sts1$^{\Delta NLS}$	
LEP632	pGEX-sts1–11,12	
HEP105	pGEX-Rpn11	
LEP601	pET28-Rpn11	
LEP603	pET28-Srp1	
LEP604	pET28-srp1–31 (S116F)	
LEP605	pET28-srp1–49 (E145K)	
LEP666	pET28-Sts1	
LEP667	pET28-sts1–2	
LEP668	pET28-sts1$^{\Delta NLS}$	
LEP669	pET28-sts1–11,12	
LEP689	pGEX-Srp1	
LEP690	pGEX-srp1–31	
LEP691	pGEX-srp1–49	
LEP703	pOC9 derivative of P_{CUP1}-Ura3-HA-SL17	R. Kulka and T. Ravid

integrated derivatives of GFP-tagged proteasome subunits were generously provided by Dr. C. Enenkel (Humboldt University). All the amplified DNAs were verified by sequencing both strands. A list of yeast strains and plasmids is shown in Tables 1 and 2, respectively.

Growth Assays and Sensitivity to Temperature—Yeast cultures were grown in selective medium and normalized to an absorbance at A_{600} of ~1. 10-Fold serial dilutions were spotted on agar plates and incubated at 23 and 37 °C.

Pulse-Chase Measurement of Protein Stability—Protein stability measurements were performed as described previously (20). We used the EXPRE^{35}S^{35}S protein labeling reagent (PerkinElmer Life Sciences) to metabolically label *STS1* and *sts1-2* expressing FLAG-Sts1 and FLAG-sts1-2, respectively. Following incubation for 5 min at 30 °C, labeling was terminated by the addition of cycloheximide, and aliquots were withdrawn at 0, 10, 30, and 60 min. Equal amounts of trichloroacetic acid-insoluble material was incubated with anti-FLAG M2-agarose beads. The samples were resolved by SDS-PAGE and exposed to x-ray film.

Native PAGE—Measurement of peptidase activity of proteasomes was examined in a native polyacrylamide gel, as described previously (20). Protein lysates (50 μg) were separated in a native gel that was overlaid with buffer containing LLVY-AMC[2] in the presence of 0.05% SDS. The fluorescence signal was detected with Kodak GelLogic Imager.

Purification of Recombinant Proteins and in Vitro Binding Assay—Expression of proteins from pGEX and pET28 vectors was achieved in *Escherichia coli* BL21S cells in the presence of 1 mM isopropyl 1-thio-β-D-galactopyranoside. Cells were lysed (in 50 mM Tris-HCl, pH 7.5, 150 mM NaCl, 5 mM Na-EDTA, 1% Triton X-100, and protease inhibitor mixture), and total protein lysate was applied to glutathione-Sepharose to purify GST-tagged proteins. Protein expression levels were determined before performing binding studies. Bacterial lysates that contained His_6-tagged proteins were mixed with purified GST proteins for 4 h at 4 °C. The unbound proteins were removed by four washes in lysis buffer. The bound proteins were released in SDS gel loading buffer, separated in 10 or 12% SDS-Tricine/PAGE, and examined by immunoblotting.

Immunoprecipitation/Immunoblotting—Yeast cells were suspended in buffer A (50 mM HEPES, pH 7.5, 150 mM NaCl,

[2] The abbreviations used are: LLVY-AMC, Leu-Leu-Val-Tyr-7-amino-4-methylcoumarin; CP, catalytic (20 S) particle; GST, glutathione S-transferase; NLS, nuclear localization signal; Tricine, *N*-[2-hydroxy-1,1-bis(hydroxymethyl)ethyl]glycine.

5 mM EDTA, and 1% Triton X-100) containing protease inhibitors (Roche Applied Science) and lysed by glass bead disruption. Protein extracts were normalized using the Bradford method (Bio-Rad) and incubated with anti-FLAG-M2-agarose. The bound proteins were released in SDS gel loading buffer, separated in 10 or 12% SDS-Tricine/PAGE, and characterized by immunoblotting. The signals were quantified using Kodak GelLogic Imaging software.

Fluorescence Microscopy—500 μl of yeast cells were pelleted, washed with 1 ml of phosphate-buffered saline (PBS), and suspended for 10 min in 100 μl of PBS containing 10 ng of 4,6-diamidino-2-phenylindole (DAPI). DAPI was removed following several washes with PBS, and the cells were then suspended in 30 μl of PBS. Cells (3 μl) were spotted on Poly-Prep slides (Sigma) and examined using a Zeiss Imager M1 microscope. All exposures were for 600 ms for GFP (filter set 38 HE) and 75 ms to detect DAPI fluorescence (filter set 49). The scale bar represents 5 μm. Zeiss AxioVision software was used for quantifying the GFP fluorescence intensity. Between five and eight different fields of view were examined, and ~50–200 cells were analyzed. Standard mean value were collected by densitometry and plotted, and Student's *t* test was applied for comparisons.

Ultrasonic Cell Disruption—Yeast were grown to exponential phase at 23 °C, suspended in medium that was prewarmed to 37 °C, and incubated for 5 h. Yeast cells were collected by brief centrifugation and washed with ice-cold buffer A (lacking Triton X-100), and 500 μl was placed in each of six microcentrifuge tubes. Each sample was exposed to varying durations of ultrasonication at 23 kHz using a horn tip diameter of 0.3 cm (Sonic Dismembrator, model 100, Fisher). The generator power setting (4) was identical for all treatments, and the duration of sonication is indicated in the figure. Following sonication, an aliquot was examined by microscopy to check the integrity of the cells and to visualize GFP localization. A 400-μl aliquot was centrifuged at 12,000 × *g*, and 50 μl of the supernatant was placed in a 96-well plate, in duplicate. GFP fluorescence was detected using a Tecan Infinite F-200 plate reader (using a filter set $\lambda_{exe} = 485$ nm; $\lambda_{em} = 535$ nm). Experimental data were collected from four independent studies, and relative fluorescence values with standard deviations were calculated.

Cell Fractionation—Yeast cells were grown at 23 °C and then transferred to 37 °C for 4 h. Cells were centrifuged at 3,000 × *g*, and the cell pellets were suspended in pretreatment buffer (50 mM Tris-HCl, pH 7.5, 10 mM $MgCl_2$, 1 M sorbitol, 60 mM 2-mercaptoethanol). Following 15 min of incubation at room temperature, the cells were pelleted (1,500 × *g*), and suspended in digestion buffer (3 ml/g, pretreatment buffer containing 5 mM 2-mercaptoethanol) that contained zymolyase 20T (2 mg/g cells). The suspension was incubated at 23 °C for 40 min, and the spheroplasts were pelleted at 4 °C (4,000 × *g*). To prepare crude nuclei, the spheroplasts were suspended in digestion buffer (0.5 ml/g) and lysed by adding dropwise into 20 volumes of cold lysis buffer (18% Ficoll, 10 mM Tris-HCl, pH 7.5, 20 mM KCl, 5 mM $MgCl_2$, 5 mM 2-mercaptoethanol, 1 mM EDTA, 1 mM PMSF, 2 μM E64, 1 μg/ml chymostatin) with continuous mixing. Cell debris and unlysed cells were removed by centrifugation at 3,000 × *g*. The supernatant was centrifuged at 20,000 × *g* for 20 min to separate the cytoplasm from the enriched nuclear pellet. Protein concentration of the supernatant (representing cytosolic fraction) was determined, and an equal amount (15 μg) was examined by immunoblotting. The pellet, representing crude nuclei, was weighed and suspended in 30 μl/mg SDS-gel electrophoresis buffer. Equal amount of protein (45 μl) was resolved by SDS-PAGE.

Antibodies—Polyclonal antibodies against Rpt1, Rad23, Dsk2, and Cdc31 were generated at Pocono Rabbit Farm and Laboratory, Inc. (Canadensis, PA). Anti-Rpn12 was a gift from Dr. D. Skowyra (Washington University, St. Louis) Antibodies against ubiquitin, FLAG-HRP, and FLAG-M2 beads were from Sigma. Anti-His_6 monoclonal antibody was purchased from Boston Biochem. Monoclonal anti-HA was obtained from Roche Applied Science. Glutathione-Sepharose 4B was from GE Healthcare.

Reagents—Suc-Leu-Leu-Val-Tyr-AMC (LLVY-AMC) was purchased from Boston Biochem. DAPI was purchased from Sigma. Enhanced chemiluminescent (ECL) reagents were from PerkinElmer Life Sciences, and the signals were detected using a Kodak GelLogic 1500 Imaging System.

RESULTS

Proteasomes Are Structurally Intact in sts1-2—We showed previously that proteasomes in *sts1-2* failed to efficiently bind multiubiquitinated proteins (17). We separated proteasomes in a native polyacrylamide gel to determine whether stability or function was altered. Separation using a native in-gel assay permits resolution of cellular proteasomes and its intermediates and can provide a qualitative assessment of both assembly and peptidase activity (20, 21). Protein extracts were characterized from *STS1* and *sts1-2* strains grown at the permissive (23 °C) and nonpermissive (37 °C) temperatures (Fig. 1*A*). We also separated extracts prepared from *rpn11-1*, which has a severe defect in proteasome assembly (20, 22). The intact 26 S proteasome contains a single catalytic 20 S particle (CP) and two regulatory (19 S) particles (1). This large 2.3-MDa complex migrates slowly in the native gel (RP2CP), and its position can be distinguished from the free catalytic 20 S particle (CP), which is indicated in Fig. 1*A*, *right margin*. In the presence of low levels of detergent (0.05% SDS), the peptidase activity of both 26 S and 20 S proteasomes is detected using a fluorogenic assay. Fig. 1*A* shows that high levels of free 20 S CP, but low levels of intact proteasomes (RP2CP), are detected in *rpn11-1* (compare ratio of RP2CP/CP in *lanes 1* and *2*). The levels of 26 S and 20 S complexes were similar in *STS1* and *sts1-2*, at both permissive (Fig. 1*A*, *lanes 3* and *4*) and nonpermissive temperatures (*lanes 5* and *6*), demonstrating that proteasomes are assembled, and equally active in *STS1* and *sts1-2*. However, this finding did not explain the cause of the growth and proteolytic defects of *sts1-2* or the inability of proteasomes to efficiently bind multiubiquitinated proteins (17).

Defects of sts1-2 Are Linked to Instability of sts1-2 Protein—We examined the stability of Sts1 and sts1-2 proteins by *in vivo* labeling with [^{35}S]methionine. FLAG-Sts1 was expressed

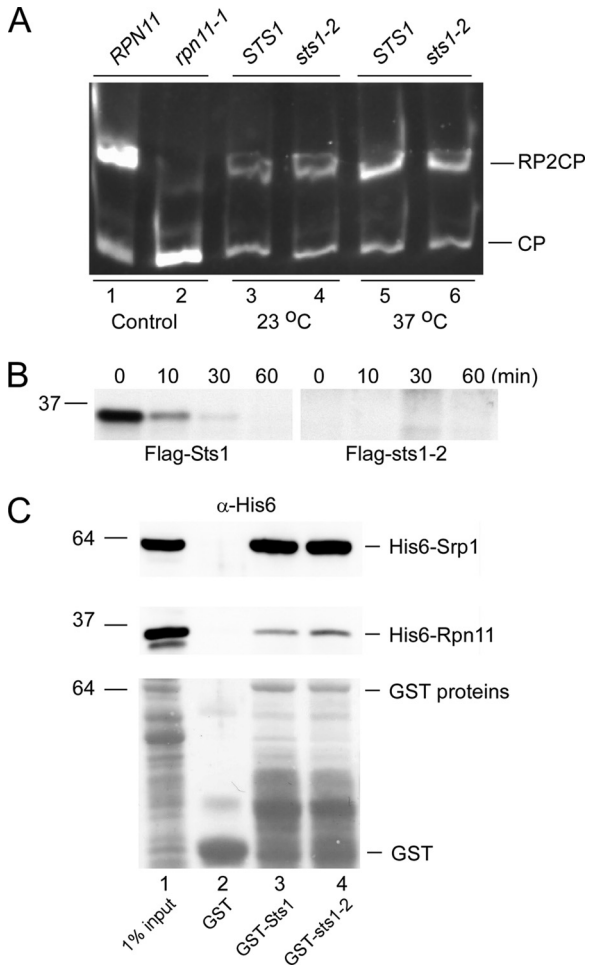

FIGURE 1. **Proteasome are assembled and functional in *sts1-2*.** *A*, protein lysates were resolved in a native polyacrylamide gel and incubated with proteasome substrate LLVY-AMC. The positions of intact 26 S proteasome (*RP2CP*) and the free CP are indicated on the *right*. In a control strain, increased proteasome dissociation in *rpn11-1* is indicated by the high levels of CP (*lane 2*). Lysates prepared from *STS1* and *sts1-2* cells that were grown at 23 and 37 °C were examined (*lanes 3–6*). *B, in vivo* stability of FLAG-Sts1 and FLAG-sts1-2 was determined by metabolic labeling with [^{35}S]methionine. Cells were grown at 23 °C and then incubated at 37 °C for 4 h prior to labeling. Following 5 min of labeling, cells were transferred to chase medium, and samples were withdrawn at the times indicated in minutes. Equal amount of TCA-insoluble protein was immunoprecipitated and examined by autoradiography. *C, in vitro* interaction of GST-Sts1 and GST-sts1-2 with His_6-Srp1 and His_6-Rpn11 was tested by immunoblotting. His_6-Srp1 and His_6-Rpn11 proteins did not bind the control GST protein. Sts1 and sts1-2 interacted with both His_6-Srp1 and His_6-Rpn11.

in *STS1* and found to be extremely unstable (Fig. 1*B*) (17), displaying an *in vivo* half-life of less than 5 min. Significantly, FLAG-sts1-2 was undetectable (in *sts1-2*), even after prolonged exposure, suggesting very rapid degradation. Sts1 is essential for viability, and the instability of sts1-2 could underlie the growth and proteolytic defects of the *sts1-2* mutant. To determine whether this mutant protein was capable of binding its partners, we purified GST-Sts1 and GST-sts1-2 from *E. coli*. Both proteins were expressed efficiently, indicating that the sts1-2 protein is not prone to aggregation, or precipitation. The GST-tagged proteins were incubated with recombinant His_6-Srp1 and His_6-Rpn11. Both GST-Sts1 and GST-sts1-2 formed equivalent interactions with Srp1 and Rpn11 (Fig. 1*C, lanes 3* and *4*), and no interaction was detected with control beads containing GST (*lane 2*). GST-Sts1 and GST-sts1-2 formed a strong interaction with His_6-Srp1 and a weaker but reproducible interaction with His_6-Rpn11. We conclude that the defect of sts1-2 *in vivo* is the result of its rapid degradation and is not due to its inability to bind physiological partners.

Proteasomes Are Mislocalized in sts1-2—Because Sts1 can bind a nuclear transport protein (Srp1), as well as a subunit in the proteasome (Rpn11) (Fig. 1*C*) (19), we investigated if it functioned as an adaptor that linked the proteasome to the nucleus. We integrated derivatives of several proteasome subunits as fusions to the green fluorescent protein (GFP) in *STS1* and *sts1-2*. Rpn1-GFP and Rpn11-GFP are subunits in the regulatory (19 S) particle, and Pre6-GFP is a subunit in the catalytic (20 S) particle. Enenkel *et al.* (2, 23) previously showed that these chimeras were expressed at physiological levels and assembled into mature proteasomes. The GFP fusions proteins are fully functional, because they can replace essential proteasome subunits. In preliminary studies, yeast cells were grown at the semi-permissive temperature (30 °C) and examined by fluorescence microscopy. We determined that Rpn1, Rpn11, and Pre6 were co-localized with the nucleus in *STS1* (data not shown). DAPI treatment showed that the GFP signal overlapped with the nucleus.

STS1 and *sts1-2* cells were transferred to fresh medium and grown at the permissive temperature (23 °C) for 1.5 and 5 h. The subcellular distribution of Rpn1-GFP in *STS1* and *sts1-2* was investigated by fluorescence microscopy (Fig. 2*A*). Both *STS1* and *sts1-2* showed strong overlap of the GFP signal with nuclei at 23 °C. However, even at 23 °C, we observed higher cytosolic levels of Rpn1-GFP in *sts1-2*. Nonetheless, it is likely that adequate levels of proteasomes are present in the nucleus in *sts1-2* to permit survival at 23 °C, the permissive temperature.

STS1 and *sts1-2* cells were transferred to 37 °C and examined at the intervals shown (Fig. 2*B*). Significant mislocalization of proteasomes was evident in *sts1-2* by 3 h, and specific nuclear staining was strongly reduced at 5 h (Fig. 2*B, lower panels*). GFP signal in the cytosol was ~2-fold higher in *sts1-2*. The GFP staining pattern in *STS1* after transfer to 37 °C was essentially unchanged (1.5 h at 37 °C), although a significant loss in nuclear GFP was evident in *sts1-2*. After 5 h incubation at 37 °C, the GFP staining in nuclear and cytoplasmic regions in *sts1-2* was indistinguishable, suggesting significant cytoplasmic localization of proteasomes. It is possible that low levels of proteasomes remain bound to nuclei at 37 °C in *sts1-2* but cannot be distinguished from the background of mislocalized cytosolic Rpn1-GFP.

Nuclear Localization Defect of sts1-2 Is Reversible—*STS1* and *sts1-2* cultures that were examined in Fig. 2*B* were transferred from 37 to 23 °C to determine whether the proteasome targeting defect of *sts1-2* was reversible. Fluorescence microscopy showed that proteasome targeting to the nucleus was restored in *sts1-2* (Fig. 2*C*). This result demonstrates that the temperature-sensitive localization defect is reversible for at least 5 h. In contrast, continued incubation of *sts1-2* at 37 °C resulted in the accumulation of large cells, which showed significant depletion of nuclear proteasomes. Because protea-

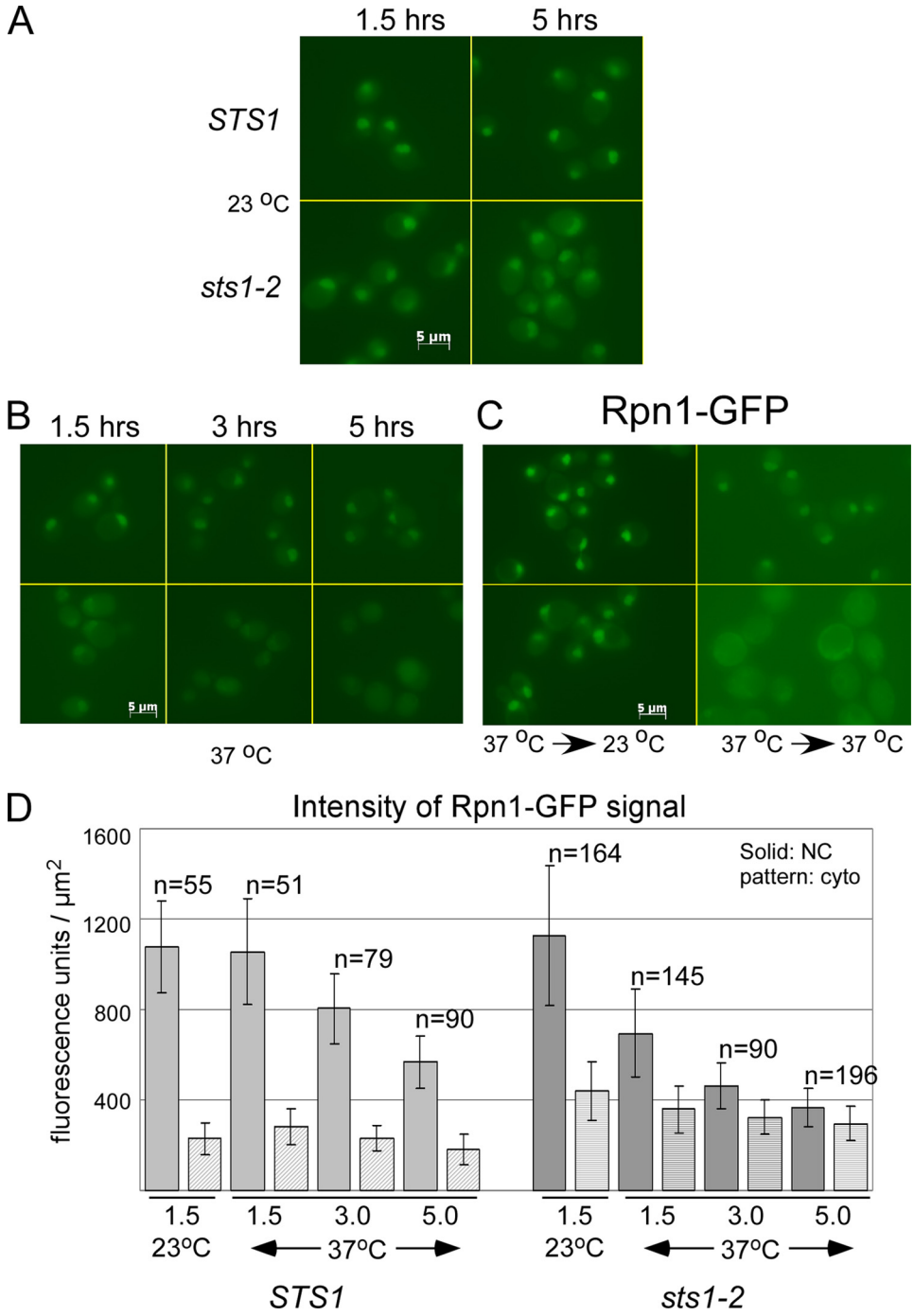

FIGURE 2. **A nuclear localization defect in *sts1-2*.** Rpn1-GFP was integrated in *STS1* and *sts1-2* at the chromosomal loci and expressed at physiological levels. *A,* actively growing cells were diluted into fresh medium and incubated at 23 °C and viewed by immunofluorescence at the times indicated. *B,* aliquot from the same cultures was transferred to medium at 37 °C, and samples were examined at the times indicated. *C,* following incubation for 5 h at 37 °C, *STS1* and *sts1-2* were diluted and incubated for ~15 h in fresh medium at either 23 or 37 °C to test for reversibility of the defect. *D,* Zeiss imaging software was used to quantify the pixel density of the images seen in the microscopy images. A minimum of five independent viewing fields were examined, and well separated cells were quantified for both cytosolic (*cyto*) and nuclear compartment (*NC*). The numbers (*n*) represent the sum of individual cells that were viewed. The standard deviation is shown.

somes are intact and functional in *sts1-2* (Fig. 1*A, lane 6*), we propose that the proteolytic defect of *sts1-2* stems from its failure to efficiently target proteasomes to the nucleus. These data were quantified using Zeiss densitometry software using multiple fields of view (Fig. 2*D*).

Proteasome Targeting Defect of sts1-2 Is Suppressed by Sts1—To confirm that the reduced level of nuclear proteasomes was a result of a defect in the sts1-2 protein, we transformed *sts1-2* (expressing Pre6-GFP) with a plasmid expressing wild type Sts1. As expected, proteasomes were inefficiently targeted to nuclei in *sts1-2* (Fig. 3*A*) after incubation at 37 °C for 4 h. However, expression of FLAG-Sts1 fully reversed this translocation defect, and the signals from GFP and DAPI were co-localized. These results confirmed that the proteasome

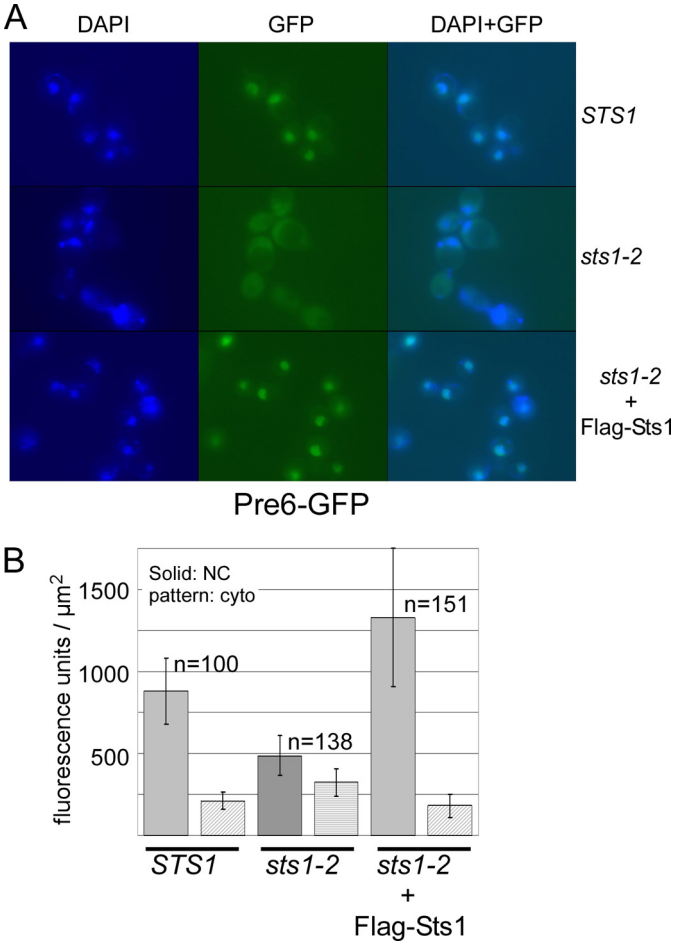

FIGURE 3. **Proteasome translocation defect of *sts1-2* is fully suppressed by plasmid-encoded Sts1.** *A,* high copy plasmid expressing FLAG-Sts1 was transformed into *sts1-2,* and the localization of integrated Pre6-GFP was examined at 37 °C. The localization defect is evident in *sts1-2*. However, this defect was completely rescued by expression of FLAG-Sts1. DAPI staining of the nuclei showed that the Pre6-GFP signal was predominantly co-localized to the nucleus. *B,* microscopy data were quantified (*n*, the number of cells quantified), and complete rescue of the trafficking defect of *sts1-2* was confirmed.

translocation defect is specifically associated with the *sts1-2* mutant. Rescue of the localization defect of *sts1-2* by Sts1 was also verified by examining the subcellular distribution of other GFP-tagged proteasome subunits (data not shown). Because the temperature-sensitive growth defect of *sts1-2* is overcome by FLAG-Sts1 (17), we conclude that cell growth is linked to the nuclear targeting of proteasomes. The microscopy data were quantified, and the results reinforced our findings (Fig. 3*B*). Intriguingly, the GFP staining intensity in *sts1-2*, expressing Sts1 from a high copy plasmid, showed ~50% more proteasomes in the nucleus than in the wild type cell.

Sts1 Overexpression Increases Nuclear Localization of Proteasomes—The results shown in Fig. 3 suggested that Sts1 levels might be limiting. Moreover, Sts1 in *Saccharomyces cerevisiae* (Fig. 1*B*) (17) and Cut8 in *Schizosaccharomyces pombe* (24) are both highly unstable proteins, raising the possibility that Sts1 abundance might influence proteasome localization. To explore this idea, we overexpressed Sts1 in wild type (*STS1*) cells from a high copy plasmid, using the copper-inducible P_{CUP1} promoter. Expression was induced by adding $CuSO_4$ directly to the growth medium. In comparison with "vector-only" control (that contained 200 μM $CuSO_4$), we determined that by increasing the levels of Sts1 nuclear localization of Pre6-GFP was appreciably elevated, even without addition of $CuSO_4$ (Fig. 4*A*). The addition of 50 μM $CuSO_4$ to the culture medium further increased GFP localization to the nucleus. However, providing 200 μM $CuSO_4$ had no additive effect on the levels of nuclear proteasomes. The quantified data (Fig. 4*B*) showed that the nuclear targeting of proteasomes was noticeably increased by higher levels of Sts1. Statistical analysis showed that the difference between vector-alone and plasmid-encoded Sts1 (0 μM $CuSO_4$) was significant ($p < 0.001$). A further increase in nuclear localization of Pre6-GFP occurred in the presence of 50 μM $CuSO_4$ (0–50 μM $CuSO_4$; $p < 0.007$). Expressing higher levels of Sts1 (200 μM $CuSO_4$) resulted in very low levels of GFP fluorescence in the cytosol, suggesting complete nuclear localization of proteasomes. Similar results were observed when we tracked a different proteasome subunit (Rpn1-GFP; data not shown). We immunoprecipitated FLAG-Sts1 from whole cell extracts and confirmed that the addition of $CuSO_4$ increased the expression of Sts1. Sts1 was also higher in the absence of $CuSO_4$ because the gene is expressed from a high copy plasmid. Higher levels of FLAG-Sts1 were detected when $CuSO_4$ was added to the medium (Fig. 4*C,* 50 μM). Addition of 200 μM $CuSO_4$ did not increase FLAG-Sts1 levels significantly (beyond the level seen with 50 μM $CuSO_4$), consistent with the nuclear targeting data (Fig. 4*A*). Sts1 interaction with the proteasome was confirmed by the co-precipitation of Rpt1. Yeast expressing only vector (*V*) showed no precipitation of Rpt1, although a faint cross-reaction with the immunoglobulin heavy chain is detected (Fig. 4*C*, *asterisk*). These results suggest that the nuclear targeting of proteasomes is influenced by the availability of Sts1, as its overexpression increased nuclear targeting and depleted proteasomes from the cytosol.

Sts1 Forms Independent Interactions with Srp1 and Rpn11—Sts1 performs an important role in the ubiquitin/proteasome pathway (17). We speculate that its interaction with the proteasome subunit Rpn11 is related to its function in the ubiquitin/proteasome system (Fig. 1*C*). Sts1 interaction with Srp1 was proposed to function in nucleocytoplasmic trafficking (19). We note that *srp1-49* has a defect in protein degradation that is suppressed by high levels of Sts1 (19). This finding suggested to us that Srp1 might be functionally linked to Rpn11, through their mutual interactions with Sts1. We speculated that Srp1/Sts1 and Sts1/Rpn11 interactions might guide the translocation of proteasomes to the nucleus. Therefore, the protein degradation defect of *srp1-49* could be due to reduced levels of nuclear proteasomes (18). To investigate if Srp1 and Rpn11 competed for binding to Sts1, we simultaneously added both His_6-Srp1 and His_6-Rpn11 to immobilized GST-Sts1. The binding reactions contained a fixed amount of His_6-Rpn11 and increasing amounts of His_6-Srp1. We found that GST-Sts1 interaction with His_6-Rpn11 was unaffected by the amount of His_6-Srp1 that was present (Fig. 5*A,* compare *lane 1* with *lane 4*). These results are consistent with the interpre-

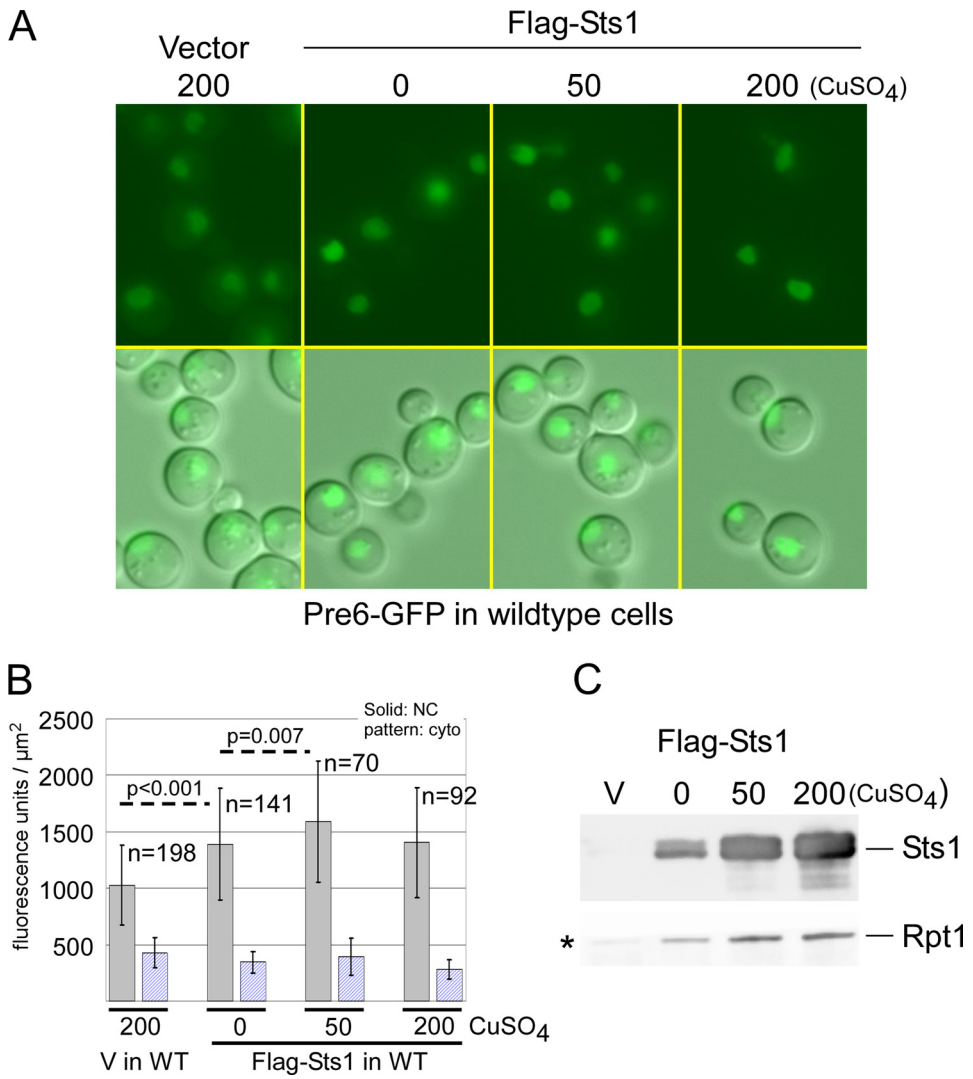

FIGURE 4. **High expression of Sts1 increases the level of nuclear proteasomes.** *A*, empty vector or the same vector overexpressing FLAG-Sts1 was transformed into *STS1*. Actively growing yeast cells were grown with or without the addition of copper sulfate to the medium. The amount of $CuSO_4$ added is indicted at the *top* of each panel. *Upper panels* show the localization of Pre6-GFP, and the *lower panels* show a merged image of GFP + differential contrast microscopy. *B,* fluorescence images were quantified, and the number of cells examined is indicated (*n*). *Dark-shaded columns* represent nuclear staining (*NC*), and *light-shaded columns* indicate cytosolic GFP levels (*cyto*). *C,* expression level of FLAG-Sts1 in the presence of 0, 50, and 200 μM $CuSO_4$ was determined by immunoprecipitation. The level of proteasome subunit Rpt1 that was co-purified with FLAG-Sts1 was also determined. A faint band detected in the vector lane (*V*) is a nonspecific reaction against the immunoglobulin heavy chain (*asterisk*).

tation that Srp1 and Rpn11 bind distinct regions in the Sts1 protein. Furthermore, prior binding of Sts1 to Rpn11 did not improve or interfere with subsequent interaction with Srp1 (data not shown). Similarly, the Sts1/Srp1 interaction did not affect Sts1 binding to Rpn11. We recognize that these data do not exclude the possibility that the interactions might represent separate complexes with Sts1. No binding was detected with GST control beads (Fig. 5*A, lane 5*).

NLS in Sts1 Is Required for Interaction with Srp1—To further characterize these interactions, we immobilized GST-Sts1 and mutant derivatives on glutathione-Sepharose beads and tested their interaction with purified His_6-tagged Srp1 and Rpn11 (Fig. 5*B*). Following a 3-h incubation at 4 °C, the unbound proteins were removed, and the bound proteins were released into SDS-containing buffer and resolved by SDS-PAGE. Consistent with earlier results, no binding was detected with GST (Fig. 5*B, lane 2*), and Sts1 and sts1-2 formed comparable interactions with both His_6-Srp1 and His_6-Rpn11 (Fig. 5*B, lanes 3* and *4*). However, because sts1-2 is highly unstable *in vivo* (Fig. 1*B*), its interaction with Srp1 and Rpn11 is expected to be significantly reduced under physiological conditions.

We investigated if the NLS in Sts1 was required for its interaction with Srp1. We incubated recombinant His_6-Srp1 and His_6-Rpn11 with immobilized sts1 mutants, including GST-$sts1^{\Delta NLS}$ (Fig. 5*B, lane 5*). We confirmed that an Sts1 mutant lacking the NLS ($sts1^{\Delta NLS}$) does not bind Srp1 (*lane 5*) (19). In contrast, another Sts1 mutant (sts1–11,12) formed efficient interactions with both Srp1 and Rpn11 (Fig. 5*B, lane 6*). Although $sts1^{\Delta NLS}$ also failed to bind Rpn11 (Fig. 5*B, lane 5*), we suspected this interaction was adversely affected by the presence of GST. Moreover, Tabb *et al.* (19) had previously described a direct interaction between Sts1 and Rpn11.

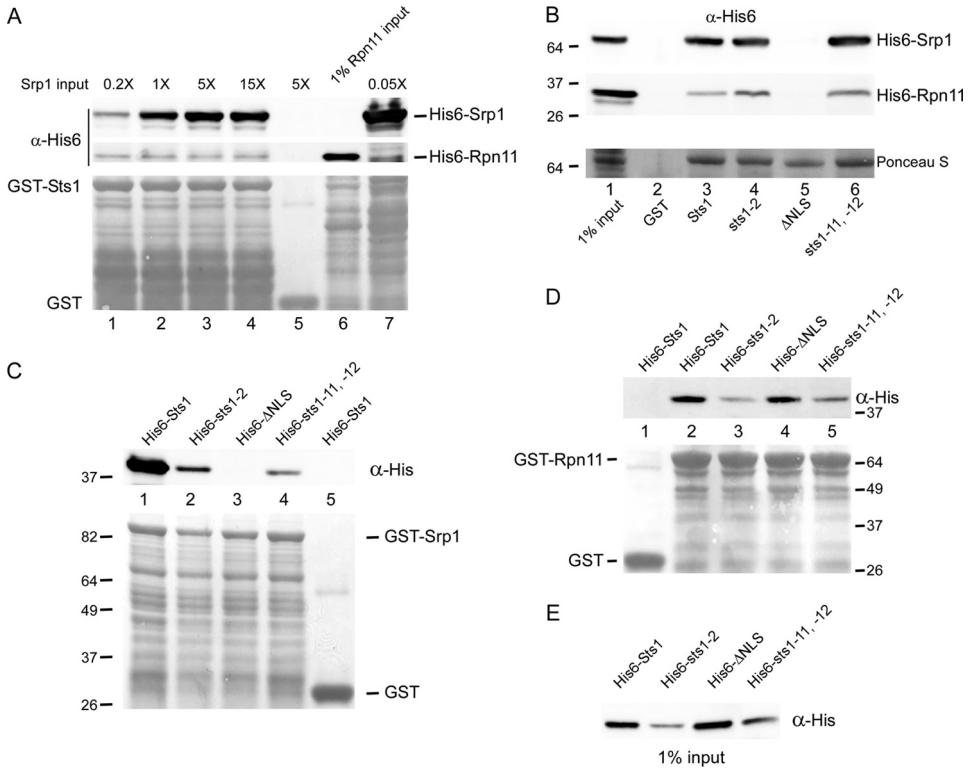

FIGURE 5. **NLS in Sts1 contributes to its function.** *A*, interaction between GST-Sts1 and both His_6-Srp1 and His_6-Rpn11 was examined. GST-Sts1 was immobilized on glutathione-Sepharose, and bacterial lysates containing a fixed amount of His_6-Rpn11 and increasing amounts of His_6-Srp1 were added. Following incubation for 4 h at 4 °C, the unbound proteins were removed, and the proteins bound to GST-Sts1 were detected by immunoblotting. Direct interaction between GST-Sts1 and both His_6-Srp1 and His_6-Rpn11 was confirmed (*lane 1*). No interaction was observed with the control GST beads (*lane 5*). Addition of increasing amounts of His_6-Srp1 did not affect Sts1 interaction with Rpn11 (*lanes 2–4*). However, higher amounts of His_6-Srp1 led to increased interaction with GST-Sts1 (compare *lanes 1* and *4*). *B,* in a complementary binding study, GST-tagged Sts1 and mutant derivatives were immobilized on glutathione-Sepharose and incubated with His_6-Srp1 and His_6-Rpn11, as described in *A*. Both Sts1 and sts1-2 formed equivalent interactions with His_6-Srp1 and His_6-Rpn11. Ponceau S staining of the nitrocellulose filter confirmed equal amounts of the GST-Sts1 proteins on the matrix. Removal of the nuclear localization signal from Sts1 (GST-$sts1^{\Delta NLS}$) prevented interaction with His_6-Srp1 and His_6-Rpn11 (*lane 5*). As noted previously, we observed no interactions with the GST control beads (*lane 2*). *C,* in a reciprocal experiment, GST-Srp1 was immobilized on glutathione-Sepharose and combined with His_6-Sts1 (*lane 1*), His_6-sts1-2 (*lane 2*), and His_6-$sts1^{\Delta NLS}$ (*lane 3*). GST-Srp1 interaction with another mutant, sts1-11,12 was also examined (*lane 4*). Nonspecific interaction between GST and His6-Sts1 was not observed (*lane 5*). His_6-$sts1^{\Delta NLS}$ was unable to bind GST-Srp1 (*lane 3*), consistent with the results in *B*. The weaker interaction between GST-Srp1 and His_6-sts1-2 is due to lower expression levels of sts1-2 in *E. coli* (see *E*). *D,* we also immobilized GST-Rpn11 on glutathione-Sepharose and examined its interaction with His_6-Sts1 and mutant derivatives. Consistent with previous data, GST-Rpn11 interacted with His_6-tagged Sts1, sts1-2, sts1–11,12, and $sts1^{\Delta NLS}$, although no interaction was detected with control GST beads. *E,* expression levels of the various Sts1/sts1 proteins in *E. coli* is shown.

Further evidence of a role for the Sts1 NLS is shown in Fig. 5*C*. GST-Srp1 was immobilized and incubated with recombinant His_6-Sts1 and various mutant derivatives. As expected, His_6-$sts1^{\Delta NLS}$ failed to bind GST-Srp1 (Fig. 5*C, lane 3*). His_6-sts1-2 and His_6-sts1-11,12 formed weak interactions with GST-Srp1 (Fig. 5*C, lanes 2* and *4*), proportional to their lower expression in *E. coli* (Fig. 5*E*). The interactions were specific because incubation of His_6-Sts1 with GST showed no binding. Collectively, these studies show that the nuclear localization of proteasomes is reduced by preventing Srp1 interaction with Sts1 ($sts1^{\Delta NLS}$).

We performed a reciprocal experiment in which recombinant GST-Rpn11 was immobilized on glutathione-Sepharose and incubated with His_6-Sts1, His_6-sts1-2, His_6-$sts1^{\Delta NLS}$, and His_6-sts1-11,12. All four proteins formed interactions with GST-Rpn11 (Fig. 5*D, lanes 2–5*), demonstrating that the NLS in Sts1 is not required for binding Rpn11. The expression level of the various His_6-tagged proteins indicates that the interaction with Rpn11 is proportional to the amount of the Sts1 proteins available in *E. coli* extracts (Fig. 5*E*).

NLS in Sts1 Is Required for Targeting Proteasomes to the Nucleus—The ability of mutant sts1 proteins to suppress the temperature-sensitive growth defect of *sts1-2* was assessed at 23 and 37 °C. Sts1 and sts1-11 (19) suppressed the growth defect of *sts1-2* at 37 °C (Fig. 6*A, lower panels*). However, $sts1^{\Delta NLS}$ was unable to support growth of *sts1-2* at 37 °C. Because $sts1^{\Delta NLS}$ is unable to bind Srp1, we speculate that its inability to suppress *sts1-2* is due to a proteasome translocation defect. We therefore examined the distribution of Pre6-GFP (Fig. 6*B*) and found that the proteasome localization deficiency of *sts1-2* was not suppressed by $sts1^{\Delta NLS}$. In contrast, Sts1 fully suppressed this proteasome translocation defect. The quantified data (Fig. 6*C*) showed that *STS1* containing vector and *sts1-2* expressing Sts1 from a low copy (CEN) plasmid had equivalent levels of nuclear proteasomes. In contrast, expression of $sts1^{\Delta NLS}$ was indistinguishable from *sts1-2* containing only vector. We conclude that the failure of $sts1^{\Delta NLS}$ to bind Srp1 underlies the inefficient nuclear localization of proteasomes and demonstrates the importance of Sts1/Srp1 interaction for cell viability.

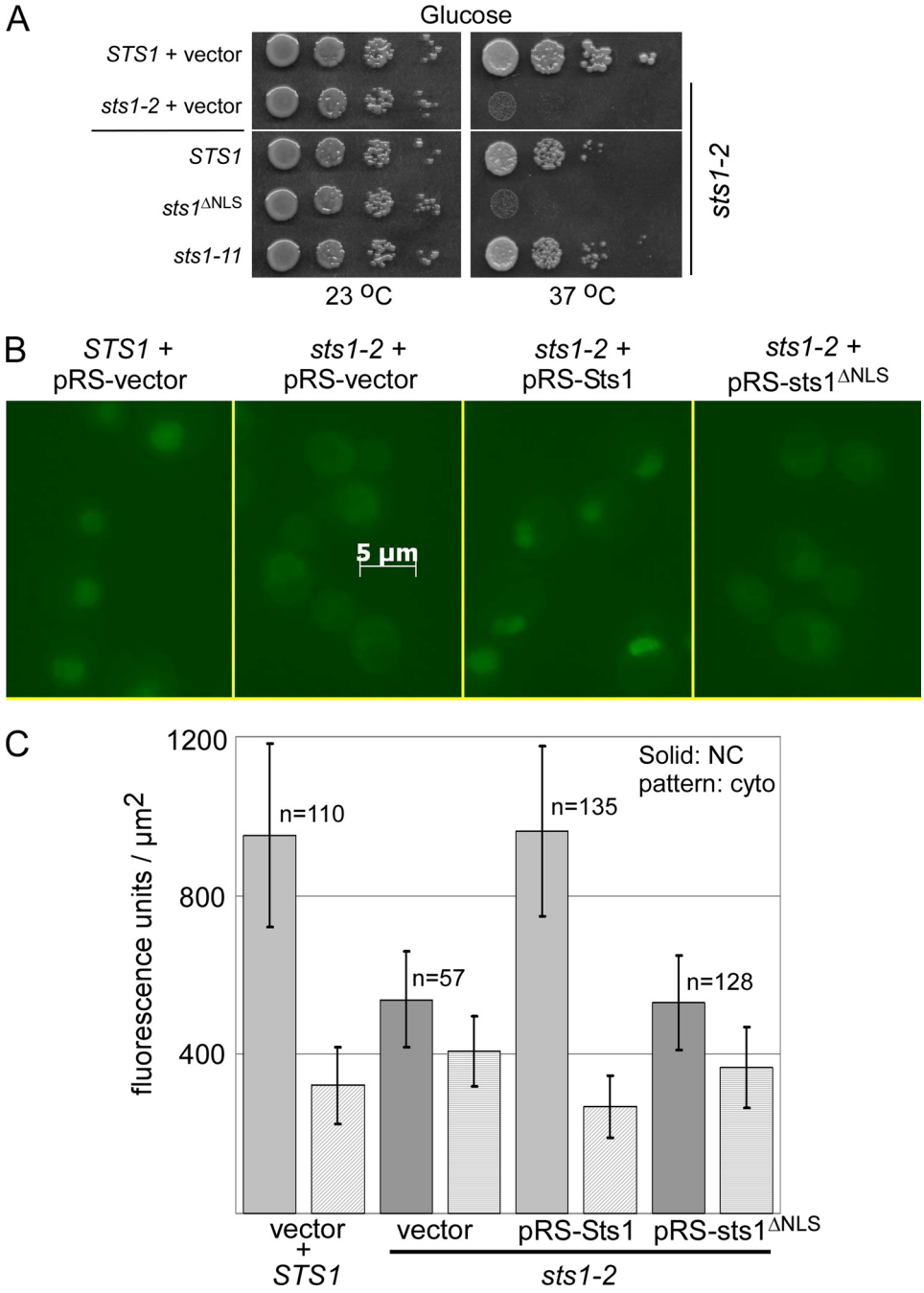

FIGURE 6. **Growth deficiency of *sts1-2* is closely linked to its proteasome targeting defect.** *A,* ability of *sts1* mutants to suppress the temperature-sensitive growth defect of *sts1-2* was determined. Plasmids expressing Sts1, sts1$^{\Delta NLS}$, and sts1-11 were transformed into *sts1-2*. Yeast cultures were adjusted to a density of $A_{600} = 1$, and 10-fold serial dilutions were spotted onto agar medium that was incubated at either 23 or 37 °C. The temperature sensitivity of *sts1-2* is compared with the wild type strain (both expressing vector) in the *upper two lanes*. *B,* to examine the requirement of the NLS in Sts1 for targeting proteasomes to the nucleus, we transformed *sts1-2* with empty vector or plasmids expressing either Sts1 or sts1$^{\Delta NLS}$. Proteasome localization was restored by Sts1 but not sts1$^{\Delta NLS}$, as indicated by the localization of Pre6-GFP. *C,* suppression of the targeting defect of *sts1-2* by Sts1 was quantified. Expression of Sts1 from the pRS vector showed proteasome localization was indistinguishable from the wild type strain (*STS1* + vector). sts1$^{\Delta NLS}$ did not overcome the proteasome mislocalization defect of *sts1-2*.

Rapid Release of Cytoplasmic Proteasome from sts1-2 Cells—To quantify the higher levels of proteasomes in the cytosol of *sts1-2,* we rapidly lysed cells by sonication (30). This approach can permit rupture of the cell wall and membrane, without disrupting nuclear integrity. We co-expressed Rpn1-GFP in *sts1-2* with either an empty plasmid or the same plasmid expressing FLAG-Sts1. We also expressed the nuclear pore protein Nup49-GFP, and the cytosolic reporter GFP in *STS1*, to provide a way to monitor the efficiency of cell lysis. The localization of both these proteins was predicted to be unaffected in *sts1-2*. Yeast cells were grown to exponential phase and transferred to pre-warmed medium at 37 °C. Following 5 h of incubation at the nonpermissive temperature (37 °C), the cells were pelleted and lysed by brief pulses of ultrasonication. Examination of the cells post-sonication showed that overall morphology and nuclear integrity remained intact (Fig. 7*A*).

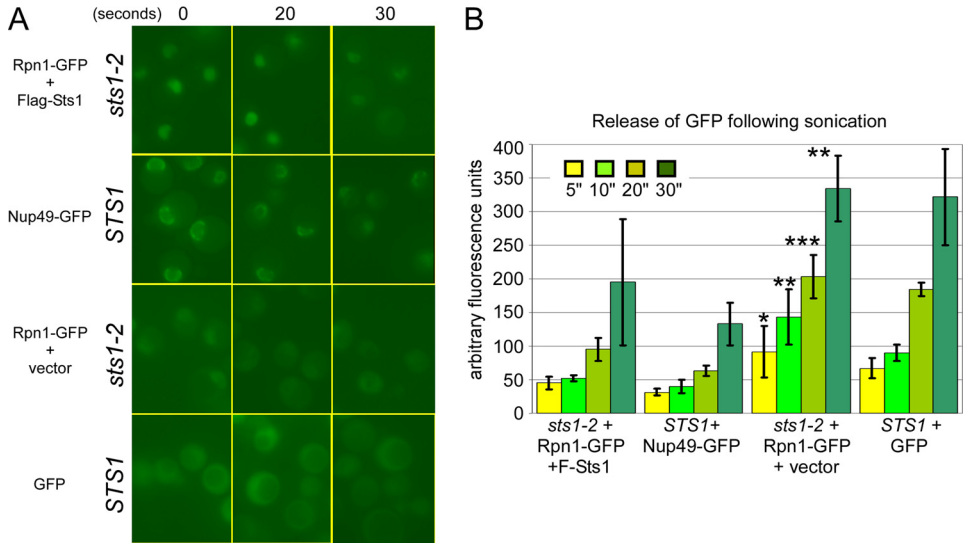

FIGURE 7. **Rapid release of a GFP-tagged proteasome subunit from *sts1-2* following ultrasonic disruption.** *A*, *STS1* expressing GFP or Nup49-GFP, and *sts1-2* co-expressing Rpn1-GFP + FLAG-Sts1, or Rpn1-GFP + empty vector were exposed to 23-kHz ultrasonic pulses (for 5, 10, 20, and 30 s). Strong nuclear localization of Rpn1-GFP is evident in *sts1-2* expressing FLAG-Sts1, even after brief ultrasonic treatment (5 s). Similarly, the nuclear localization of Nup49-GFP (seen as a fluorescent ring circumscribing the nucleus) was unaffected after a 5-s pulse. The mislocalization of proteasomes (Rpn1-GFP) is *sts1-2* resembles the cytosolic localization of GFP in *STS1* (compare the *two lower rows*). Cells were also imaged at all time points to monitor cell morphology and integrity. Prolonged sonication (>60 s) resulted in complete cell lysis and release of both nuclear (Nup49-GFP/Rpn1-GFP) and cytosolic proteins (GFP; data not shown). *B*, cells were pelleted after sonication, and duplicate aliquots of the supernatant were withdrawn, and GFP fluorescence was measured using a fluorescence plate reader. Rpn1-GFP, Nup49-GFP, and GFP were detected in the extracellular medium following sonication. The data representing duplicate measurements, from four independent experiments, are plotted. The error bars represent standard deviation measurements (*, $p < 0.05$; **, $p < 0.01$; ***, $p < 0.001$).

After 20 s of sonication, proteasomes were still localized to the nuclei in *sts1-2* expressing FLAG-Sts1, and similarly, Nup49-GFP was detected in the nuclear envelope in *STS1*. Following each ultrasonic pulse, cells were pelleted, and the supernatant was examined for the release of GFP-Rpn1 (Fig. 7*B*). We found that in wild type cells (*sts1-2* expressing FLAG-Sts1), Rpn1-GFP was detected in the medium only after 20 s of continuous sonication. Similarly, nuclear integrity was unaffected following shorter pulses of treatment (as determine by microscopy and the retention of Nup49-GFP in the cells). The release of Nup49-GFP into the medium was not observed until the cells had been treated for >30 s. In striking contrast, higher levels of GFP-Rpn1 were released from *sts1-2* into the medium following 5 s of treatment. As expected, cytosolic GFP was also rapidly released from *STS1*, providing strong support for the hypothesis that mislocalized proteasomes in *sts1-2* accumulate in the cytosol. It is also significant that the values measured from four independent experiments offer very robust statistical confirmation of this hypothesis. Cell fractionation studies also lend support for this model (supplemental Fig. 1). Whole cell extracts were partitioned into cytosolic and crude nuclei fractions and characterized by immunoblotting. Higher levels of proteasome subunits were detected in the cytosol of *sts1-2*.

srp1 Mutant Is Defective in Nuclear Translocation of Proteasomes—Of two *srp1* mutants characterized by Tabb *et al.* (19) (*srp1-31* S116F; *srp1-49* E145K), only *srp1-49* had a defect in protein degradation. This mutant was subsequently reported to mislocalize proteasomes at the nonpermissive temperature (18). We predicted that if Sts1/Srp1 interaction promoted nuclear translocation of proteasomes, then an srp1 mutant protein that is deficient in binding Sts1 would also have lower levels of nuclear proteasomes. We therefore examined srp1-31 and srp1-49 interactions with Sts1. GST-Srp1, GST-srp1-31, and GST-srp1-49 were bound to glutathione-Sepharose and incubated with His_6-Sts1 (Fig. 8*A*). The bound protein was identified by immunoblotting and quantified (Fig. 8*B*). Although higher levels of GST-srp1-49 were present on the Sepharose beads, ~3-fold lower amounts of His_6-Sts1 were co-purified (Fig. 8*B, lane 5*). His_6-Sts1 formed similar interactions with GST-Srp1 and GST-srp1-31 (Fig. 8*A, lanes 3* and *4*). In a reciprocal experiment, recombinant His_6-Srp1, His_6-srp1-31, and His_6-srp1-49 were incubated with immobilized GST-Sts1 (Fig. 8*C*). Although equal amounts of His_6-tagged Srp1, srp1-31, and srp1-49 were present on the matrix, His_6-srp1-49 showed reproducibly reduced interaction with GST-Sts1 that was confirmed by densitometry (Fig. 8*D*). The proteolytic defect of *srp1-49* could be caused by reduced proteasome integrity and function or by poor nuclear localization. To address this, we examined total protein extracts in a native in-gel assay and found that proteasomes were fully active in *srp1-49*, and the assembly resembled the wild type strain (Fig. 8*E*).

The distribution of proteasomes was examined in *SRP1*, *srp1-49,* and *srp1-31* using Rpn1-GFP. The level of nuclear proteasomes was reduced in *srp1-49* but not as significantly in *srp1-31* (Fig. 9*A*), consistent with the previously reported protein degradation defect of *srp1-49* (19). It is significant in this regard that srp1-49, but not srp1-31, showed reduced binding to Sts1 (Fig. 8*A*). The fluorescence data were quantified (Fig. 9*B*) and showed reduced nuclear staining intensity in *srp1-49*. Nuclear GFP staining in *SRP1* was ~2-fold higher than in *srp1-49*, consistent with reduced nuclear localization in the mutant. A trend toward lower nuclear localization was also

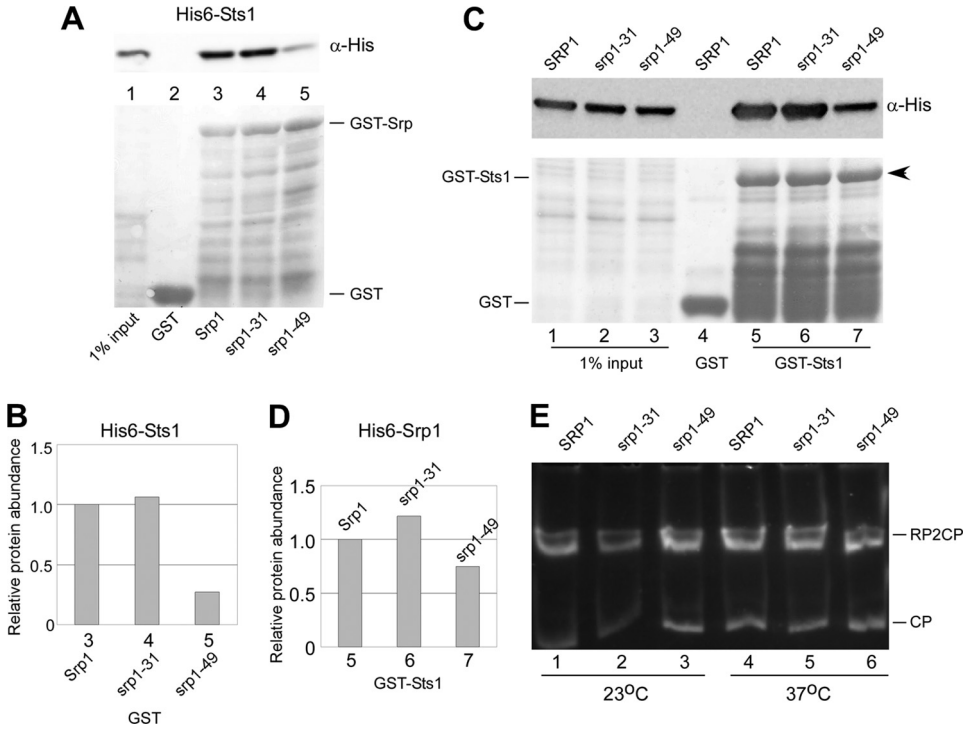

FIGURE 8. **srp1-49 shows reduced binding to Sts1.** *A,* GST-tagged Srp1 and mutant derivatives were immobilized and incubated with *E. coli* extracts containing His_6-Sts1. Binding was examined by immunoblotting. Both Srp1 and srp1-31 formed equivalent interactions with His_6-Sts1, although srp1-49 showed reduced binding. No interaction was detected with the control GST beads. *B,* binding results in *A* were quantified by densitometry, and ~3-fold lower amounts of His_6-Sts1 were co-precipitated with GST-srp1-49. *C,* in a reciprocal assay GST-Sts1 was immobilized and incubated with His_6-tagged forms of Srp1/srp1. *Lanes 1–3* show that equivalent amounts of Srp1, srp1-31, and srp1-49 were present in *E. coli* extracts. However, following incubation with GST-Sts1, lower amounts of His_6-srp1-49 were purified, consistent with the previous results. No interaction was detected with GST control beads. *D,* binding results in *C* were quantified by densitometry, and lower interaction between Sts1 and srp1-49 was observed. *E,* protein extracts were prepared from *SRP1*, *srp1-31*, and *srp1-49* and separated in a native polyacrylamide gel. The gel was incubated with proteasome substrate *Suc*-LLVY-AMC, and the fluorescence signal from AMC (released by chymotryptic activity of the proteasome) was detected. The positions of the intact 26 S proteasome (*RP2CP*) and the catalytic core particle (*CP*) are shown at both 23 and 37 °C. The slight increase in the levels of free CP in *srp1-49* at 23 °C is not significant.

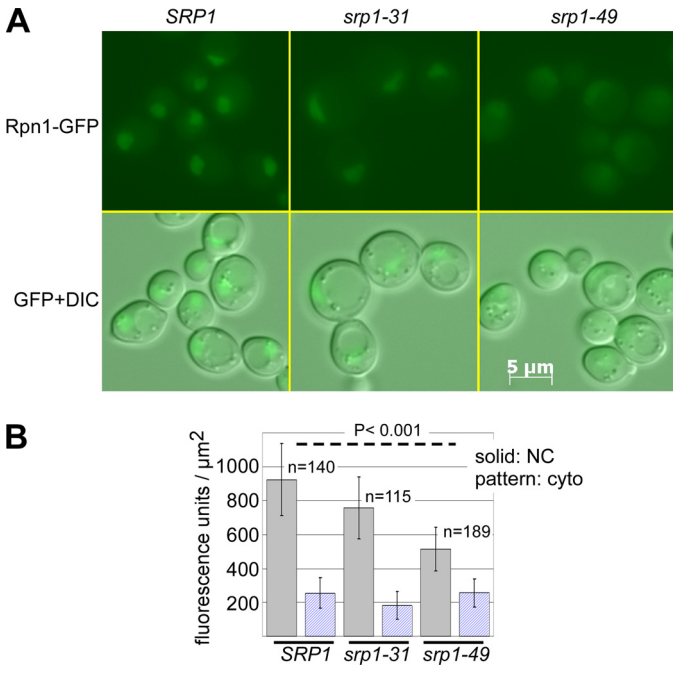

FIGURE 9. ***srp1* mutant displays defective proteasome localization.** *A*, Rpn1-GFP was detected by immunofluorescence, and defective nuclear targeting of proteasomes was observed in *srp1-49*. The defect was less severe in *srp1-31*. *B,* fluorescence signals were quantified, and significant decreases in nuclear staining ($p < 0.001$) were evident in *srp1-49* compared with the *SRP1* wild type strain.

evident in *srp1-31*, although the data were not statistically robust. In contrast, proteasome mislocalization in *srp1-49* was highly significant ($p < 0.001$). We propose that Srp1 stimulates protein degradation by binding Sts1 and recruiting proteasomes to the nucleus.

Sts1 Restores Nuclear Targeting of Proteasomes in rad23Δ rpn10Δ—Rad23 translocates ubiquitinated proteins to the proteasome (9). Rpn10 represents a major proteasome receptor for multiubiquitinated proteins (11). We reported previously that the loss of both Rad23 and Rpn10 (*rad23Δ rpn10Δ*) caused pleiotropic growth and proteolytic defects (16), revealing a functional link between these proteins (16). The defects of *rad23Δ rpn10Δ* were suppressed by high levels of Sts1 (17). Although Rad23 and Rpn10 can bind proteasomes and multiubiquitinated proteins (25, 26), we determined that Sts1 only interacts with the proteasome (17). This finding suggested that Sts1 did not suppress *rad23Δ rpn10Δ* by functionally replacing either Rad23 or Rpn10.

We investigated the subcellular distribution of proteasomes in *rad23Δ rpn10Δ*. A DNA construct expressing Rpt1-GFP was integrated in *rad23Δ rpn10Δ*, and the subcellular distribution of the GFP signal was examined in actively growing cells at 18 °C (which is a semi-permissive temperature for *rad23Δ rpn10Δ*). Proteasomes were significantly mislocalized (Fig. 10*A*). However, expression of Sts1 from the galactose-inducible P_{GAL1} promoter restored localization of protea-

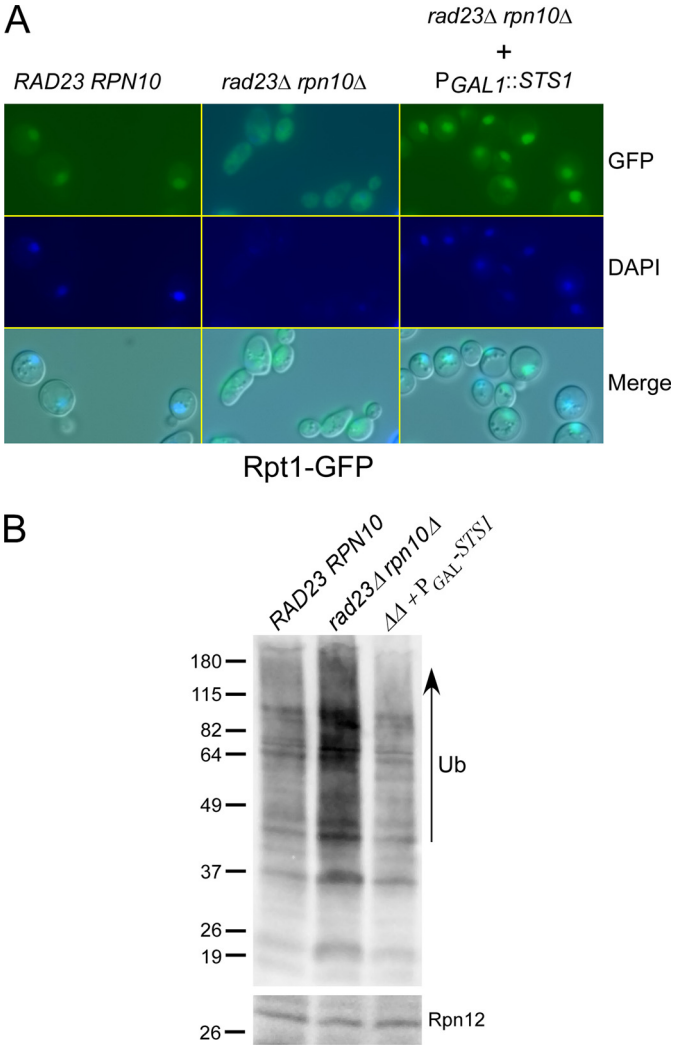

FIGURE 10. **Sts1 can suppress the proteasome localization defect of *rad23Δ rpn10Δ*.** *A,* Rpt1-GFP was integrated in wild type and *rad23Δ rpn10Δ* strains and grown at a semi-permissive temperature (18 °C). Fluorescence imaging showed defective nuclear targeting of proteasomes in *rad23Δ rpn10Δ*. Expression of P_{GAL1}::*STS1* in *rad23Δ rpn10Δ* restored nuclear localization of Rpt1-GFP, showing full suppression of this targeting defect. DAPI staining of nuclei in *rad23Δ rpn10Δ* is difficult due to the highly aberrant cell morphology of this mutant. However, a merged image of GFP + differential interference contrast microscopy shows clear co-localization of the Rpt1-GFP signal with DAPI. *B,* proteolytic defects of *rad23Δ rpn10Δ* include stabilization of substrates and accumulation of multiubiquitinated proteins (*2nd lane*). Overexpression of Sts1 restored normal levels of ubiquitinated (*Ub*) proteins in *rad23Δ rpn10Δ* (*3rd lane*) to the levels detected in the wild type strain (*1st lane*). Overexpression of Sts1 did not affect the abundance of proteasomes, as indicated by the levels of Rpn12 (*lower panel*).

somes to the nucleus in *rad23Δ rpn10Δ*. Quantification of these data is difficult because of the aberrant cell morphology of *rad23Δ rpn10Δ* and the high levels of nuclear fragmentation and cell death. As seen in Fig. 10*A*, DAPI staining was poor in *rad23Δ rpn10Δ*.

We showed previously that high levels of multiubiquitinated proteins accumulated in *sts1-2* (17). This defect intensified when the cells were incubated at the nonpermissive temperature. Similarly, the levels of multiubiquitinated proteins increased in *rad23Δ rpn10Δ* (16). Based on our findings that proteasomes are mislocalized in *rad23Δ rpn10Δ* and *sts1-2*, we questioned if restoring nuclear targeting of proteasomes re-established normal levels of multiubiquitinated proteins. We prepared protein extracts from wild type (*RAD23 RPN10*) and *rad23Δ rpn10Δ* (Fig. 10*B*) and examined the effect of overexpressing Sts1. Equal amounts of protein were separated and immunoblotting showed that normal levels of multiubiquitinated proteins were detected when Sts1 was overexpressed in *rad23Δ rpn10Δ*. The abundance of the proteasome (indicated by Rpn12) was unaffected. One interpretation of this result is that by successfully restoring proteasome targeting to the nucleus, Sts1 re-established the efficient turnover of nuclear substrates in *rad23Δ rpn10Δ*. Further study will be required to test the idea that defective proteasome targeting in *rad23Δ rpn10Δ* interferes with the degradation of nuclear proteins and accounts for the pleiotropic defects of this double mutant.

Turnover of a Nuclear Protein Is Reduced in sts1-2—A simple prediction of our findings is that nuclear substrates should be stabilized if proteasomes are inefficiently targeted to the nucleus in *sts1-2*. We tested this hypothesis by expressing Clb2-HA at physiological levels in *STS1* and *sts1-2*. Protein extracts were prepared from cells grown at 23, 30, and 37 °C (Fig. 11*A*). Equal amount of protein was resolved by SDS-PAGE and examined by immunoblotting. We found that Clb2-HA levels were increased in *sts1-2*, at all three temperatures. The levels of Clb2-HA were standardized to the abundance of Rpn12 (Fig. 11*B*). The quantified results indicated that Clb2-HA levels increase >3-fold in *sts1-2* at 37 °C. The same extracts were also incubated with antibodies against the HA epitope to immunoprecipitate Clb2-HA. Higher levels were recovered from *sts1-2* at all three temperatures (Fig. 11*C*). Fig. 11*C, lane 6,* showed evidence for higher molecular weight derivatives of Clb2-HA, consistent with the accumulation of multiubiquitinated Clb2 in *sts1-2*. A longer exposure of this filter showed clear evidence for higher molecular weight forms of Clb2-HA (Fig. 11*D, arrow*). The filter shown in Fig. 11*D* was subsequently probed with antibodies against ubiquitin. In agreement with the aforementioned results, the high molecular weight species detected with anti-HA antibodies appear to represent multiubiquitinated forms of Clb2-HA (Fig. 11*E, arrow*). Total extracts were also examined, and as we showed previously (17), the levels of multiubiquitinated proteins increased in *sts1-2* at all temperatures examined (supplemental Fig. 2).

Increased Turnover of a Cytosolic Substrate in sts1-2—The prediction that nuclear proteins should be stabilized in *sts1-2* is supported by the results in Fig. 11 (17). However, it was unclear if the failure of proteasomes to localize to the nucleus in *sts1-2* would affect the turnover of cytosolic substrates. Testing this idea is not straightforward because few proteins have been clearly shown to be degraded by the proteasome in the cytosol. We avoided examining proteins linked to endoplasmic reticulum-associated degradation because in *S. cerevisiae* the endoplasmic reticulum membrane is closely associated with the nuclear envelope. We therefore examined the turnover of an engineered substrate, Ura3-SL17 (28). This substrate contains Ura3-HA with a carboxyl-terminal extension that promotes rapid turnover, without involvement of the endoplasmic reticulum. Ura3-SL17 was expressed in *STS1* and *sts1-2,* and growth on synthetic medium lacking uracil

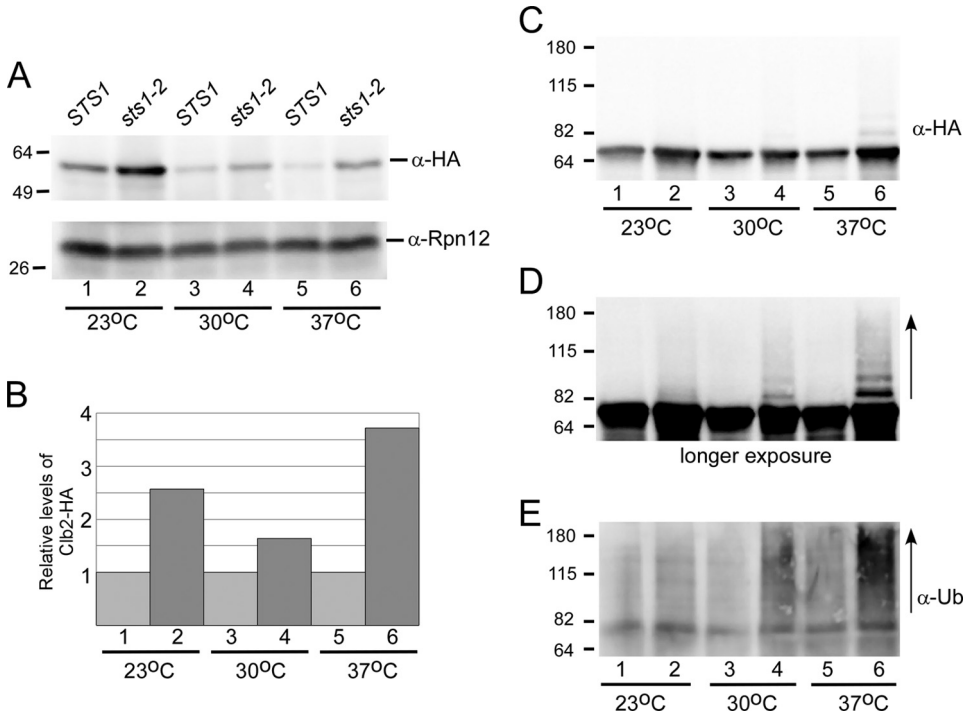

FIGURE 11. **Stabilization of a ubiquitinated protein in *sts1-2*.** *A,* gene expressing Clb2-HA was integrated in *STS1* and *sts1-2*, and extracts were prepared at 23, 30, and 37 °C. Total protein extract was examined by immunoblotting. Clb2-HA levels were elevated in *sts1-2* at all three temperatures. In contrast, the abundance of proteasome subunit Rpn12 was essentially unchanged. *B,* abundance of Clb2-HA was standardized to the level of Rpn12 by densitometry and plotted. The most significant increase was observed at the nonpermissive temperature (37 °C), consistent with the proteasome mislocalization defect of this mutant. *C,* extracts described above were incubated with antibodies against the HA epitope to purify Clb2-HA. The purified protein was examined by immunoblotting and incubation with anti-HA antibodies. Consistent with the results in *A*, we detected higher levels of Clb2-HA in *sts1-2* (*lanes 2, 4,* and *6*). *D*, longer exposure of the image shown in *C* reveals higher molecular weight forms of Clb2-HA, consistent with multiubiquitination. A temperature-specific accumulation is evident, because extracts prepared from cultures grown at 37 °C showed the highest levels (compare *lanes 5* and *6*). *E,* filter shown in *D* was stripped and reprobed with antibodies against ubiquitin, and a strong reaction was detected. As noted above, the intensity of this modification was higher at 37 °C (*lane 6*), when the proteasome trafficking defect of *sts1-2* is most severe.

was examined (Fig. 12*A*). No growth was observed in the wild type strain (*STS1*), consistent with rapid degradation of this reporter protein. Significantly, no growth was detected in *sts1-2*, demonstrating that the cytosolic degradation of Ura3-SL17 was unaffected. In contrast, growth was observed in *pre1-2 pre2-2*, which expresses a peptidase-deficient proteasome. These results demonstrate that although Ura3-SL17 degradation requires the proteasome, it does not involve Sts1. We also confirmed previous studies that showed that Ura3-SL17 degradation requires ubiquitination by the Ubc6 and Ubc7 ubiquitin-conjugating enzymes (28).

Based on these findings, we examined the steady-state abundance of Ura3-SL17 (Fig. 12*B*). Total extracts were examined by immunoblotting, and we detected very low levels of Ura3-SL17 in *STS1* and *sts1-2* (Fig. 12*B, lanes 1* and *2*), as well as in *pre1-1 pre2-2* (*lane 3*). Stabilization of Ura3-SL17 was more easily observed in *ubc6*Δ *ubc7*Δ, consistent with previous reports (Fig. 12*B,* compare *lanes 4* and *5*). The higher basal level in these strains (Fig. 12*B, lanes 4* and *5*) is due to a different genetic background. The expression of Rad23 and Rpn12 is also shown, and their levels are similar in *STS1* and *sts1-2*. Total extracts were also examined for the levels of multiubiquitinated proteins, and high levels were detected in *pre1-1 pre2-2* (Fig. 12*B, lower panel, lane 3*), consistent with its defect in proteasome function. Higher levels were also observed in *sts1-2* (*lane 2*; and see supplemental Fig. 2). The reduced levels of ubiquitinated species in *ubc6*Δ *ubc7*Δ were not observed consistently (Fig. 12*B, lane 4*). (As noted earlier, the strains shown in Fig. 12*B, lanes 1–3* are in a different genetic background than strains in *lanes 4* and *5*).

Ura3-SL17 contains an HA epitope and was immunoprecipitated from the strains described. The purified proteins were examined by immunoblotting, using antibodies against the HA epitope (Fig. 12*C*). Consistent with the results in Fig. 12*B*, we detected very low levels of Ura3-SL17 in *sts1-2*, indicating significantly accelerated degradation. Stabilization of this substrate was observed in both *pre1-1 pre2-2* (Fig. 12*B, lane 3*) and in *ubc6*Δ *ubc7*Δ (*lane 4*). The same filter was incubated with antibodies against ubiquitin. Evidence for higher molecular weight derivatives of Ura3-SL17 is evident in the proteasome mutant (Fig. 12*C, lower panel, lane 3*). These results agree with previous reports that showed that Ura3-SL17 is degraded by the ubiquitin/proteasome system. Our findings demonstrate that the turnover of this cytosolic substrate is not prevented in *sts1-2*. Remarkably, the abundance of Ura3-SL17 actually decreased, suggesting that the higher levels of cytosolic proteasomes in *sts1-2* can accelerate turnover of cytosolic substrates.

DISCUSSION

The failure to localize proteasomes to the nucleus underlies the temperature-sensitive growth defect of *sts1-2*. The target-

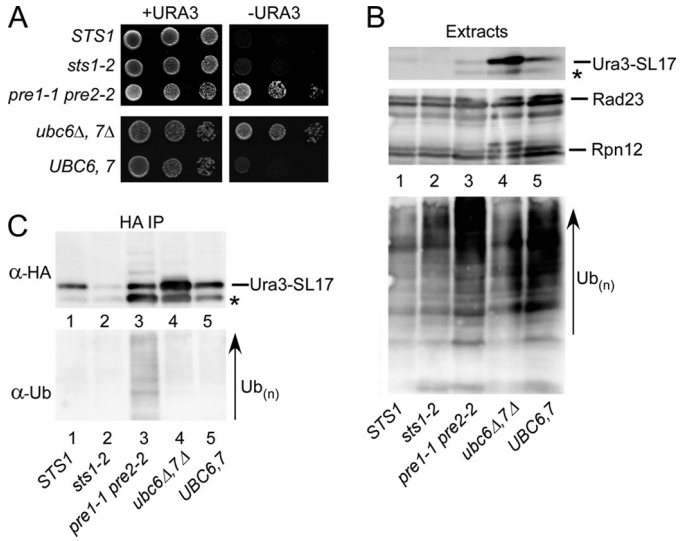

FIGURE 12. **Cytoplasmic protein degradation is not impaired in *sts1-2*.** Yeast cells that stabilize Ura3-SL17 can grow on medium lacking uracil. *A, STS1* and *sts1-2* expressing Ura3-SL17 were unable to grow on SM-uracil at a semi-permissive temperature (30 °C). However, a *pre1-1 pre2-2* proteasome mutant formed colonies on SM-ura, in agreement with previous studies. Deletion of the E2 enzymes that target Ura3-SL17 for degradation (*ubc6*Δ *ubc7*Δ) also allowed growth on SM-ura medium. *B,* we examined Ura3-SL17 abundance to verify that growth on SM-ura was the result of its stabilization. Ura3-SL17 was detected at very low levels in *STS1* and *sts1-2*, although high levels were detected in *ubc6*Δ *ubc7*Δ. The abundance of Rad23 and proteasome subunit Rpn12 was essentially similar in all the strains characterized. The filter was stripped and reprobed with antibodies against ubiquitin, and higher levels of multiubiquitinated proteins were seen in *pre1-1 pre2-2* and *sts1-2*. The stabilization of Ura3-SL17 in *ubc6*Δ *ubc7*Δ is consistent with the ability of this strain to grow on SM-ura. *C,* to improve detection, Ura3-SL17 was immunoprecipitated with antibodies against HA epitope. Ura3-SL17 was detected in *STS1* but was present at significantly lower levels in *sts1-2*, suggesting that its degradation might be accelerated by the higher levels of cytosolic proteasomes. This filter was stripped and reprobed with antibodies against ubiquitin, and a broad smear of multiubiquitin cross-reacting signal was detected in *pre1-1 pre2-2*.

ing of proteasomes to the nucleus requires an NLS in Sts1, which binds Srp1. An Sts1 mutant lacking the NLS (sts1$^{\Delta NLS}$) failed to target proteasomes to the nucleus. Because a mutation in *SRP1* (*srp1-49*, E145K) that reduced interaction with Sts1 also impaired proteasome localization, we have identified an epistatic relationship with Sts1. A key conclusion is that by binding both nuclear transport and proteasome subunits Sts1 can promote the localization of proteasomes to the nucleus.

We isolated Sts1 as a dosage suppressor of the proteolytic defects of *rad23*Δ *rpn10*Δ (17). This mutant lacks the Rad23 shuttle factor that delivers ubiquitinated proteins to the proteasome, as well as Rpn10, a proteasome receptor for ubiquitinated proteins. Proteasome integrity and function were unaffected in *rad23*Δ *rpn10*Δ, suggesting that the proteolytic defects were caused by some other deficiency. We show here that *rad23*Δ *rpn10*Δ has reduced levels of nuclear proteasomes. We determined that Sts1 could restore the levels of nuclear proteasomes in *rad23*Δ *rpn10*Δ.

Our studies showed that proteasomes are assembled and catalytically active in *sts1* mutants. The protein degradation defect of *sts1-2* (17) is closely linked to its failure to target proteasomes to the nucleus. Overexpression of Sts1 noticeably increased the levels of nuclear proteasomes (Fig. 4) while depleting proteasome levels in the cytoplasm. Overexpression of Sts1 had no effect on proteasome abundance or function, consistent with a specific role in subcellular trafficking. We propose that Sts1 is rate-limiting in this targeting mechanism, because Sts1 in *S. cerevisiae* and a related protein in *S. pombe* (Cut8) are both highly unstable (18). sts1-2 mutant protein can form normal interactions with its cellular partners (Srp1; Rpn11), but due to its rapid degradation, the levels of nuclear proteasomes are significantly diminished. The failure of sts1$^{\Delta NLS}$ to target proteosomes is mechanistically different from sts1-2, but the effect is similar. Overexpression of Sts1 increased the level of nuclear proteasomes, consistent with a previously reported role for Sts1 and Cut8 in this process (24, 27).

The significance of Srp1/Sts1 and Sts1/Rpn11 interactions was not fully understood, and it was proposed that these interactions might have different biochemical effects (19). The yeast Srp1 protein binds nuclear localization signals to translocate proteins into the nucleus. Strikingly, a mutant form of Srp1 (srp1-49) showed reduced binding to Sts1 (Fig. 8) (19) and reduced levels of nuclear proteasomes (Fig. 9) (18). We note that the nuclear translocation defect of *srp1-49* was weaker than that observed in *sts1-2*. We speculate this occurs because srp1-49 can form a weak interaction with Sts1, whereas sts1$^{\Delta NLS}$ failed to bind Srp1. Collectively, these results suggest that Sts1, Srp1, and Rpn11 represent essential components of a pathway that target proteasomes to the nucleus. The Srp1 protein (importin-α) has been characterized extensively as a central component of the nuclear import machinery. In contrast to the many factors that compose the nuclear pore, Srp1 is a soluble protein. The interaction between Srp1 and Sts1, and the resulting trafficking of proteasomes to the nucleus, raises interesting questions regarding the ultimate destination of nuclear proteasomes. Although subunits of the proteasome have been detected inside the nucleus, it is far less clear if intact and proteolytically active proteasomes exist in the nucleus. Our findings describe a key initiator step leading to the trafficking of proteasomes to the nucleus. Although our findings support the idea that proteasomes reside on the nuclear periphery, we cannot discount alternative locations, including the inner surface of the nuclear envelope.

Another line of evidence that links Sts1 to protein degradation is the effect of overexpression. High levels of Sts1 increased the levels of nuclear proteasomes in wild type, *sts1-2,* and *rad23*Δ *rpn10*Δ cells. This can explain why the proteasome localization defect of *rad23*Δ *rpn10*Δ was suppressed by overexpressing Sts1. A nuclear targeting defect is expected to cause accumulation of multiubiquitinated proteins, ultimately leading to cell death. In agreement, the levels of multiubiquitinated proteins increased in *sts1-2*, although they were not associated with proteasomes at their correspondingly high levels (17). This observation suggests that nuclear ubiquitinated proteins may accumulate when there are insufficient levels of proteasomes at the nucleus.

We showed previously that the nuclear protein Sic1 is stabilized in *sts1-2* (9). We show here that another nuclear protein, Clb2, is also stabilized in *sts1-2* and, significantly, was conjugated to multiubiquitin chains. This effect was exacerbated at 37 °C when the nuclear localization defect of *sts1-2* is most severe. Based on these findings, we conclude that nu-

clear proteins are successfully ubiquitinated in *sts1-2* but fail to bind proteasomes, because they are not targeted to the nucleus. Further study will be required to determine whether the failure to localize proteasomes to the nucleus is the immediate cause of nuclear substrate stabilization. A previous report that defective proteasomes (*cim5-1*; *cim3-1*) can be successfully delivered to the nucleus suggests that catalytic function is not required for nuclear localization (18).

Previous studies from Enenkel *et al.* (2) showed that a major fraction of proteasomes in yeast (~80%) are targeted to the nucleus. Proteasomes can be co-purified with nuclear/endoplasmic reticulum membranes, demonstrating that they are localized to the nuclear envelope (29). As noted earlier, the present studies do not ascertain if proteasomes targeted by Sts1 enter the nucleus or remain tethered to the cytoplasmic surface of nuclei.

Multiple mechanisms may co-exist to traffic proteasomes to the nucleus. Several proteasome subunits contain NLS that can promote nuclear targeting (18). Consequently, Sts1/Rpn11 interaction might not represent the sole mechanism for trafficking proteasomes. Because Srp1 is intact in cells expressing either sts1-2 or sts1$^{\Delta NLS}$, its interaction with the NLS in other proteasome subunits should be unaffected (18). However, removal of the NLS in Sts1 (sts1$^{\Delta NLS}$) caused a complete loss of nuclear proteasomes, indicating that Sts1 plays a central role in this mechanism. We propose that Sts1 either participates in a major mechanism for mobilizing proteasomes or is an essential component in multiple targeting pathways.

Although the Sts1/Rpn11 binding is weak, this interaction is reproducible, in agreement with previous two-hybrid studies (18). Sts1 interaction with Rpn11 is specific because no binding was detected with other recombinant proteasome subunits (Rpn1, Rpn8, and Rpn10; data not shown). We propose that by binding both Rpn11 and Srp1, Sts1 guides the interaction of proteasomes with the nucleus. Previous studies indicated that subcomplexes of the proteasome might be independently targeted to the proteasome (18). However, our finding show that components of both 19 S and 20 S particles are mislocalized in *sts1-2*, suggesting that intact proteasomes are targeted to the nucleus by Sts1. Whether Sts1 binds the proteasome first (via Rpn11), or Srp1 (via NLS), remains to be determined.

These studies provide insight into the mechanism for nuclear targeting of proteasomes. We propose that a tripartite interaction involving Srp1, Sts1, and Rpn11 promotes this mechanism. We reported previously that the interaction between proteasomes and multiubiquitinated proteins was significantly reduced in *sts1-2* (18). We suggest that if proteasomes are not successfully translocated to the nucleus, nuclear substrates are ubiquitinated but cannot be degraded. This idea is supported by our finding that the nuclear substrate Clb2-HA is ubiquitinated but stabilized in *sts1-2*. However, a cytoplasmic reporter protein, Ura3-SL17, was degraded more rapidly, suggesting that the availability of increased amounts of cytosolic proteasomes can accelerate the turnover of cytosolic substrates. Taken together, these findings suggest that efficient protein degradation requires adequate levels of nuclear proteasomes.

Acknowledgments—We thank Drs. Enenkel (Humboldt University), D. Skowyra (St. Louis University), M. Hoschstrasser (Yale University), R. Kulka (Hebrew University), and T. Ravid (Hebrew University) for plasmids, strains, and antibodies. We also thank Dr. Nomura for providing yeast srp1 strains and STS1 plasmids. Dr. A. Chandra and N. Torres are thanked for contributions during preliminary stages of this study, and members of the laboratory are thanked for critical review of the manuscript.

REFERENCES

1. Glickman, M. H., and Ciechanover, A. (2002) *Physiol. Rev.* **82,** 373–428
2. Enenkel, C., Lehmann, A., and Kloetzel, P. M. (1998) *EMBO J.* **17,** 6144–6154
3. Lehmann, A., Janek, K., Braun, B., Kloetzel, P. M., and Enenkel, C. (2002) *J. Mol. Biol.* **317,** 401–413
4. Garrenton, L. S., Braunwarth, A., Irniger, S., Hurt, E., Künzler, M., and Thorner, J. (2009) *Mol. Cell. Biol.* **29,** 582–601
5. Russell, S. J., Reed, S. H., Huang, W., Friedberg, E. C., and Johnston, S. A. (1999) *Mol. Cell* **3,** 687–695
6. Kim, J. H., Choi, J. K., Cinghu, S., Jang, J. W., Lee, Y. S., Li, Y. H., Goh, Y. M., Chi, X. Z., Lee, K. S., Wee, H., and Bae, S. C. (2009) *J. Cell. Biochem.* **107,** 557–565
7. Cheong, J. K., Gunaratnam, L., and Hsu, S. I. (2008) *J. Biol. Chem.* **283,** 11661–11676
8. Stewart, D., Ghosh, A., and Matlashewski, G. (2005) *J. Virol.* **79,** 8773–8783
9. Chen, L., and Madura, K. (2002) *Mol. Cell. Biol.* **22,** 4902–4913
10. Schauber, C., Chen, L., Tongaonkar, P., Vega, I., Lambertson, D., Potts, W., and Madura, K. (1998) *Nature* **391,** 715–718
11. van Nocker, S., Sadis, S., Rubin, D. M., Glickman, M., Fu, H., Coux, O., Wefes, I., Finley, D., and Vierstra, R. D. (1996) *Mol. Cell. Biol.* **16,** 6020–6028
12. Elsasser, S., Chandler-Militello, D., Müller, B., Hanna, J., and Finley, D. (2004) *J. Biol. Chem.* **279,** 26817–26822
13. Verma, R., Oania, R., Graumann, J., and Deshaies, R. J. (2004) *Cell* **118,** 99–110
14. Deveraux, Q., Ustrell, V., Pickart, C., and Rechsteiner, M. (1994) *J. Biol. Chem.* **269,** 7059–7061
15. Raasi, S., and Pickart, C. M. (2003) *J. Biol. Chem.* **278,** 8951–8959
16. Lambertson, D., Chen, L., and Madura, K. (1999) *Genetics* **153,** 69–79
17. Romero-Perez, L., Chen, L., Lambertson, D., and Madura, K. (2007) *J. Biol. Chem.* **282,** 35574–35582
18. Wendler, P., Lehmann, A., Janek, K., Baumgart, S., and Enenkel, C. (2004) *J. Biol. Chem.* **279,** 37751–37762
19. Tabb, M. M., Tongaonkar, P., Vu, L., and Nomura, M. (2000) *Mol. Cell. Biol.* **20,** 6062–6073
20. Chandra, A., Chen, L., Liang, H., and Madura, K. (2010) *J. Biol. Chem.* **285,** 8330–8339
21. Glickman, M. H., Rubin, D. M., Fried, V. A., and Finley, D. (1998) *Mol. Cell. Biol.* **18,** 3149–3162
22. Verma, R., Aravind, L., Oania, R., McDonald, W. H., Yates, J. R., 3rd, Koonin, E. V., and Deshaies, R. J. (2002) *Science* **298,** 611–615
23. Enenkel, C., Lehmann, A., and Kloetzel, P. M. (1999) *Mol. Biol. Rep.* **26,** 131–135
24. Takeda, K., and Yanagida, M. (2005) *Cell* **122,** 393–405
25. Bertolaet, B. L., Clarke, D. J., Wolff, M., Watson, M. H., Henze, M., Divita, G., and Reed, S. I. (2001) *Nat. Struct. Biol.* **8,** 417–422
26. Chen, L., Shinde, U., Ortolan, T. G., and Madura, K. (2001) *EMBO Rep.* **2,** 933–938
27. Tatebe, H., and Yanagida, M. (2000) *Curr. Biol.* **10,** 1329–1338
28. Gilon, T., Chomsky, O., and Kulka, R. G. (1998) *EMBO J.* **17,** 2759–2766
29. Yen, H. C., Espiritu, C., and Chang, E. C. (2003) *J. Biol. Chem.* **278,** 30669–30676
30. Guerrero, S., Lopez-Malo, A., and Alzamora, S. M. (2001) *Innov. Food Sci. Emerg. Technol.* **2,** 31–39